35th Annual International Conference of the IEEE EMBS
Osaka, Japan, 3 - 7 July, 2013

A Multiresolution Framework for Ultrasound Image Segmentation by Combinative Active Contours

Weiming Wang[1], Jing Qin[2], Yim-Pan Chui[1] and Pheng-Ann Heng[1]

Abstract— **We propose a novel multiresolution framework for ultrasound image segmentation in this paper. The framework exploits both local intensity and local phase information to tackle the degradations of ultrasound images. First, multiresolution scheme is adopted to build a Gaussian pyramid for each speckled image. Speckle noise is gradually smoothed out at higher levels of the pyramid. Then local intensity-driven active contours are employed to locate the coarse contour of the target from the coarsest image, followed by local phase-based geodesic active contours to further refine the contour in finer images. Compared with traditional gradient-based methods, phase-based methods are more suitable for ultrasound images because they are invariant to variations in image contrast. Experimental results on left ventricle segmentation from echocardiographic images demonstrate the advantages of the proposed model.**

I. INTRODUCTION

Ultrasound imaging has become one of the most widely used diagnostic and therapeutic tools in modern medical applications, especially for image-guided interventions and therapies. Compared with other imaging modalities, such as CT and MRI, it is more portable and versatile, and does not produce any harmful radiation. In order to improve the performance of diagnosis and treatment, reliable and automatic or semi-automatic segmentation methods are required to detect interested objects in ultrasound images. However, accurate segmentation of these images is still a challenging task due to various ultrasound artifacts, including intensity inhomogeneity, low contrast and high speckle noise.

A lot of efforts have be dedicated to enhancing ultrasound image quality and improving segmentation accuracy [1]. In early investigations, statistical analysis of speckle is studied [2] and several filtering techniques for speckle reduction are presented [3][4]. To handle intensity distortion in ultrasound images, Xiao et al. [5] proposed an expectation-maximization method that simultaneously estimates intensity distortion and segments the image into different regions. Shape knowledge is also of great interest in many applications. For example, Johan et al. [6] applied active appearance motion model (AAMM) to detect endocardial contour over the full heart cycle. However, inclusion of *a priori* shape information may lead to erroneous segmentation result if the target is deformed due to pathological changes.

[1]Weiming Wang, Yim-Pan Chui and Pheng-Ann Heng are with Department of Computer Science and Engineering, The Chinese University of Hong Kong, Shatin N.T. Hong Kong {wangwm, ypchui, pheng} at cse.cuhk.edu.hk

[2]Jing Qin is with Center for Human Computer Interaction, Shenzhen Institutes of Advanced Technology, Chinese Academy of Sciences, Shenzhen China jing.qin at siat.ac.cn

Active contour models (ACM) [7] have been widely investigated and can be broadly categorized into two classes: edge-based models and region-based models. Both the two models have been incorporated into level set framework for ultrasound image segmentation [8][9]. However, most of these models only utilize intensity or gradient information to evolve the contour, which is usually insufficient for low contrast ultrasound images. On the other hand, phase-based methods have been shown to perform well in segmenting ultrasound images. Mulet-Parada and Noble [10] first successfully used local phase information for feature detection on echocardiogram sequences, which is later extended by Rajpoot et al. [11] by computing local phase from the monogenic signal [12]. Recently, Belaid et al. [13] employed both local phase and orientation to capture the boundaries of left ventricle. However, previous phase-based methods mainly rely on edge information and are usually sensitive to initial contour because of limited capture range.

Multiresolution scheme has been demonstrated to be an efficient technique to segment ultrasound images [14]. It relies on the conversion of speckled images with Rayleigh statistics [8] to subsampled images with Gaussian statistics by building a Gaussian pyramid. Due to Gaussian smoothing and subsampling, the intensity distribution of image pixels at higher pyramid levels can be approximated as Gaussian statistics, which is far more mathematically tractable and separable than Rayleigh statistics that actually characterizes ultrasound images. In [15], Lin et al. presented a multiscale framework that combines region and edge information to segment echocardiographic image. However, this framework is based on C-V model [16] that assumes the regions to be segmented are homogeneous, and thus has limited success for images with intensity inhomogeneity.

This paper presents a novel multiresolution framework for ultrasound image segmentation. First, multiresolution scheme is adopted to build a Gaussian pyramid for each speckled image. The multiresolution scheme gradually smooths out speckle noise as well as reduces the overall computation by transferring the computing to higher pyramid levels. Then local intensity-driven active contours are employed to locate the coarse contour of the target from the coarsest image, followed by local phase-based geodesic active contours (GAC) to further evolve the contour in finer images. This modified GAC model works well for ultrasound images with low contrast and weak boundaries as phase-based methods are theoretically intensity invariant. We evaluate the performance of the proposed model on left ventricle segmentation from echocardiographic images.

978-1-4577-0216-7/13/$26.00 ©2013 IEEE

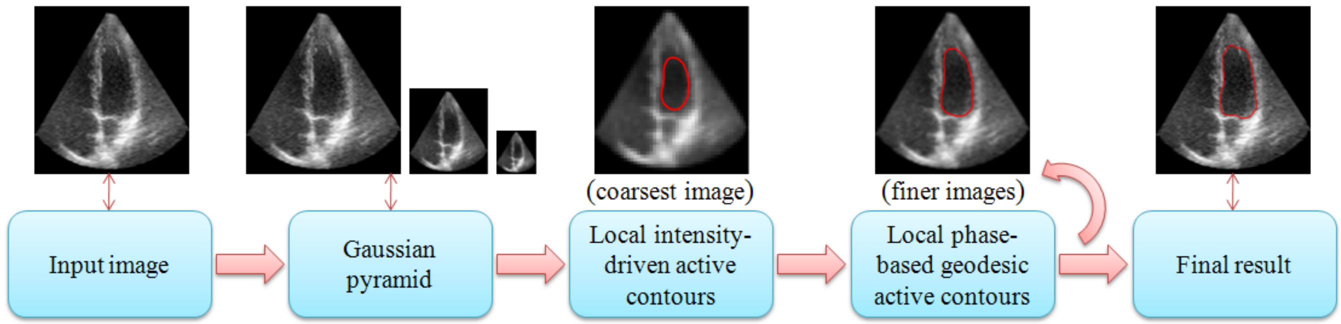

Fig. 1: Overview of the proposed model. A Gaussian pyramid is first constructed from the input image. Then the contour of left ventricle is captured progressively from high to low levels of the pyramid.

II. METHODS

Pipeline of the proposed model is shown in Fig. 1. A Gaussian pyramid is first constructed from the input image. Then the segmentation is performed in a coarse-to-fine manner where the result from a high level will be passed to next lower level as initial contour. Specifically, local intensity-driven active contours are employed to capture the coarse contour of left ventricle from the coarsest image. After that, local phase-based geodesic active contours are used to further deform the contour in finer images. The final contour is obtained after all the pyramid levels are processed.

A. Local Intensity-driven Active Contours

Let us consider an image I defined in domain $\Omega \subset \Re^2$, image segmentation is to find a contour C that partitions Ω into n different regions Ω_i, such that $\Omega = \cup_{i=1}^{n} \Omega_i, \Omega_i \cap \Omega_j = \varnothing, \forall i \neq j$. We denote $P_i = \prod_{\Omega_i} p(I(y))$ to be the probability of random field Ω_i, where $p(I(y))$ is the probability density function (PDF) of gray level $I(y)$ at pixel y. Assuming the intensity of image pixels is independently distributed, partitioning Ω corresponds to maximizing the likelihood function $\prod_{i=1}^{n} P_i$. By taking the negative logarithm operation, the maximization is turned to a minimization problem as

$$\sum_{i=1}^{n} -log(P_i) = \sum_{i=1}^{n} \int_{\Omega_i} -\log(p(I(y)))dy. \quad (1)$$

In our multiresilution framework, the intensity distribution in the coarsest image can be approximated as Gaussian statistics as explained previously. Here we adopt a Gaussian kernel with spatially varying mean and variance to model the intensity distribution within the neighborhood of pixel x as $p_x(I(y)) = \frac{1}{\sqrt{2\pi}\sigma(x)} \exp\left(-\frac{(\mu(x)-I(y))^2}{2\sigma(x)^2}\right)$, where $\mu(x)$ and $\sigma(x)$ are local intensity mean and variance, respectively. Moreover, as local energy models [17][18] usually perform better than global energy models [16] for inhomogeneous images, we incorporate another kernel function $K_\alpha(d) = \frac{1}{\sqrt{2\pi}\alpha} \exp\left(-\frac{|d|^2}{2\alpha^2}\right)$ into (1) to achieve this local property, leading to the following energy function for each pixel x

$$E_x(I, C) = \sum_{i=1}^{n} \int_{\Omega_i} -K_\alpha(x-y) \log(p(I(y)))dy, \quad (2)$$

which will be integrated over Ω to segment the whole image.

Without loss of generality, we assume the image to be partitioned into foreground and background for simplicity. These two regions can be represented as outside and inside of the zero level set of a level set function ϕ, respectively. By introducing the Heaviside function H, we obtain the following objective function to be minimized

$$F(I,\phi) = \sum_{i=1}^{2} \int\int -K_\alpha(x-y) \log(p(I(y)))M_i(\phi(y))dydx$$
$$+\mu \int \frac{1}{2}(|\nabla\phi(x)| - 1)^2 dx + \lambda \int |\nabla H(\phi(x))| dx, \quad (3)$$

where $M_1(\phi) = H(\phi)$, $M_2(\phi) = 1 - H(\phi)$ and the subscript Ω is omitted for simplification. The second term of (3) is a regularization term [19] used to penalize the deviation of the level set function from signed distance function (SDF) and the third term corresponds to the length of the contour [16]. Finally, by calculus of variations, the gradient descent flow that minimizes (3) is derived as

$$\begin{aligned}\frac{\partial\phi}{\partial t} &= \delta(\phi)(e_1 - e_2) + \mu\left(\nabla^2\phi - div\left(\frac{\nabla\phi}{|\nabla\phi|}\right)\right) \\ &+ \lambda\delta(\phi) div\left(\frac{\nabla\phi}{|\nabla\phi|}\right), \end{aligned} \quad (4)$$

where

$$e_i(x) = \int -K_\alpha(y-x)\left[\log(\sigma_i(y)) + \frac{(\mu_i(y) - I(x))^2}{2\sigma_i(y)^2}\right] dy \quad (5)$$

and δ is the Dirac function that is approximated by a smooth function $\delta_\epsilon(x) = \frac{1}{\pi}\frac{\epsilon}{\epsilon^2+x^2}$ in our experiments.

B. Local phase-based Geodesic Active Contours

Geodesic active contours (GAC) are originally proposed in [20] and the evolution equation is given by

$$\frac{\partial\phi}{\partial t} = g|\nabla\phi| div\left(\frac{\nabla\phi}{|\nabla\phi|}\right) + \nabla g \cdot \nabla\phi + \nu g|\nabla\phi|, \quad (6)$$

which relies on the gradient-based edge detector g to stop the contour at object boundaries. However, this gradient-based edge detector may produce high values in low contrast regions, and the contour will pass through weak boundaries. We solve this problem by exploiting local phase information from the monogenic signal, and design a phase-based edge detector to handle low contrast ultrasound images.

1) Monogenic Signal: To perform local analysis of 1D signal, one usually needs to construct a complex analytical signal, which is formed by taking the original signal f and its Hilbert transform f_H as real part and imaginary part, respectively. However, the Hilbert transform is only restricted for 1D function, and 2D extension of the above local analysis is usually performed by first applying 1D analysis over several orientations and then combining these 1D analyses together to provide a single measure. Recently, Felsberg and Sommer [12] proposed a 2D isotropic analytic signal, called monogenic signal. This 2D analytic signal preserves the core property of 1D analytic signal that decomposes a signal into local phase and local amplitude, and is defined by combining the original 2D signal with its Riesz transform f_R to form a 3D vector $f_M = (f, f_R) = (f, h_1 * f, h_2 * f)$, where h_1 and h_2 are the Riesz filters [21].

In practical applications, local properties are estimated via a bank of quadrature filters tuned to various spatial frequencies because real images usually consist of a wide range of frequencies. Hence a set of bandpass filters g are combined with the monogenic signal, which then can be represented as a scalar-valued even and a vector-valued odd filtered responses, i.e., $even = g * f$ and $odd = (g * h_1 * f, g * h_2 * f)$, respectively. Here the Gaussian derivative kernels are selected as bandpass filters for feature detection. In frequency domain, a 2D isotropic bandpass Gaussian derivative kernel is defined as

$$G(\omega) = n_c |\omega|^a \exp(-s^2 |\omega|^2), \tag{7}$$

where $\omega = (u, v)$. Please refer to [22] for other parameters.

2) Phase-based Edge Detector: Phase congruency model [23] postulates that features are perceived at points, where the Fourier components are maximally in phase. Various feature types give rise to points of high phase congruency, including step edges, line and roof edges, and Mach bands. Step edge detection corresponds to finding points that have phase responses near to 0 or π. In [24], Kovesi proposed to use feature asymmetry over a number of scales to detect step edge features. Inspiring from this, we define the following multiscale feature asymmetry measure

$$MSFA = \frac{\sum_n \lfloor |odd_n| - |even_n| - T_n \rfloor}{\sum_n \sqrt{odd_n^2 + even_n^2 + \varepsilon}}, \tag{8}$$

where ε is a small constant, T_s is the noise threshold and $\lfloor \cdot \rfloor$ denotes zeroing of negative values. $MSFA$ takes values between 0 (smooth regions) and 1 (boundaries).

Different from previous work, the above $MSFA$ measure is computed from the monogenic signal and thus can be applied to perform 2D local analysis directly. This property greatly simplifies the computation of local analysis for 2D signal. Furthermore, multiscale approach offers a better control on feature detection quality. Finally, the $MSFA$ measure is used to design a new phase-based edge detector, which will be incorporated into GAC model to replace the previous gradient-based edge detector, as following

$$g = \frac{1}{1 + MSFA^{\beta}}, \tag{9}$$

where β is the scale parameter. This new edge detector responds well to low contrast images as the $MSFA$ measure is independent of image intensity.

TABLE I: The mean and standard deviation (SD) of DSC measurement of the four computerized segmentation methods in ten echocardiographic images.

Methods	GAC model	Lin's Model	Wang's model	our approach
Mean (%)	87.58	90.56	88.34	95.45
SD (%)	4.82	3.13	4.48	1.81

III. EXPERIMENTS

We validate the performance of the proposed model with ten echocardiographic images. During the experiments, we use the following parameter setting. At the highest level of the pyramid, the parameters in (4) are set as μ = 1.0, λ = 0.0001 $\times$ 255 $\times$ 255. At lower pyramid levels, we use ν = -0.8, β = 0.3, and the Gaussian derivative kernels are set with wavelengths = (15, 20, 25) and bandwidth = 2 octaves. Lastly, the level set function ϕ is initialized as a binary function, taking constant values 1 and -1 in regions outside and inside of the zero level set, respectively.

Our approach is compared with three classical computerized segmentation methods: GAC model [20], Lin's model [15] and Wang's model [18]. For these three methods, we use the parameters that produce the best results. Two of the ten echocardiographic images are shown in Fig. 2. Original images with high speckle noise and low image contrast are presented in the first column and manual segmentation of the left ventricle is also displayed in the second column. Results of GAC model are shown in the third column. As can be seen, the contour is likely to pass through weak boundaries due to the use of gradient-based edge detector. Lin's model shares the same weakness as GAC model (see the fourth column). Moreover, because Lin's model relies on C-V model at the highest pyramid level, it has limited ability to handle inhomogeneous images. Results of Wang's model are presented in the fifth column. This method also cannot accurately segment left ventricle as it models the intensity distribution of ultrasound images with Gaussian statistics. In contrast, our approach precisely captures the contour of left ventricle by combining Wang's model and GAC model into a multiresolution framework, as shown in the sixth column.

Finally, TABLE I quantitatively compares the four computerized segmentation methods using the Dice similarity coefficient [25], which is defined as

$$DSC = 2 \times \frac{|S_m \cap S_c|}{|S_m| + |S_c|}, \tag{10}$$

where S_m and S_c represent the pixel sets by manual and computerized segmentation, respectively. The closer the DSC values are to 1, the higher the accuracy is. As shown in the table, our approach achieves the highest mean value and lowest SD value, indicating the superiority of the proposed model. This high accuracy and robustness also imply that our approach can be adopted to reduce the dependency of human experts in clinical applications.

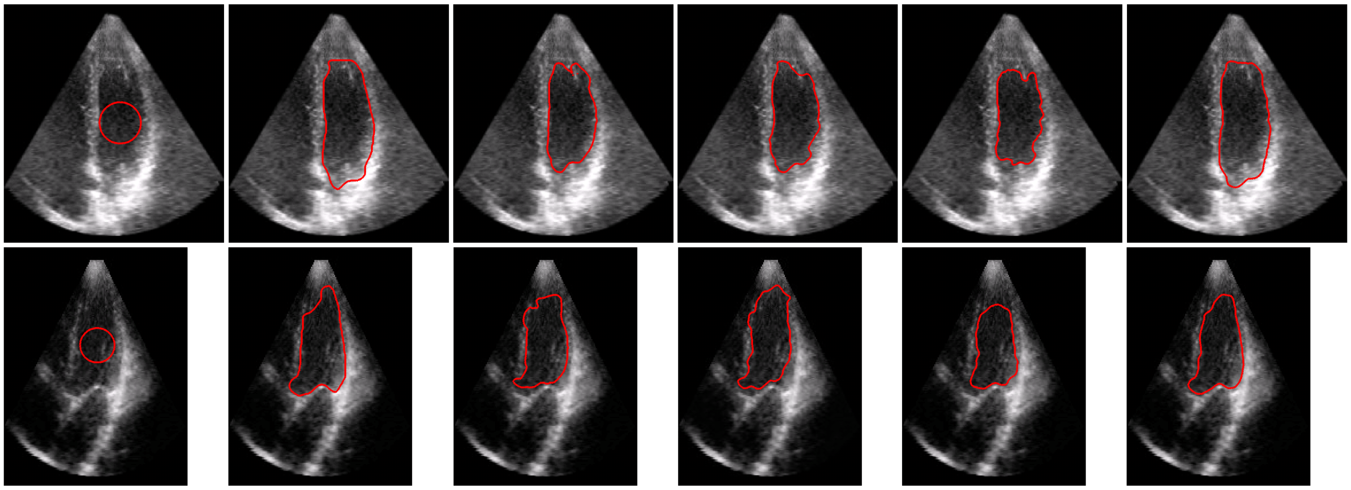

Fig. 2: Comparison of left ventricle segmentation from echocardiographic images. (First column) Original images overlaid with initial contour. (Second column) Manual segmentation. (Third column) Results of GAC model. (Fourth column) Results of Lin's model. (Fifth column) Results of Wang's model. (Sixth column) Results of our approach.

IV. Conclusions

In this paper, a novel multiresolution framework for ultrasound image segmentation is presented. Speckle noise is gradually smoothed out due to the multiresolution scheme. Furthermore, both local intensity and local phase information are exploited to deal with various ultrasound artifacts. Experimental results on left ventricle segmentation from echocardiographic images demonstrate the high accuracy and robustness of our approach. In future work, more experiments will be conducted to further evaluate the reliability of the proposed model.

Acknowledgment

The work described in this paper was supported by a grant from the Research Grants Council of Hong Kong (Project No. CUHK 412510) and a grant from the National Science Foundation of China (Project No. 61233012).

References

[1] J. A. Noble and D. Boukerroui, "Ultrasound image segmentation: a survey," *IEEE Trans. Med. Imag.*, vol. 25, no. 8, pp. 987–1010, 2006.

[2] R. Wagner, S. Smith, J. Sandrik, and H. Lopez, "Statistics of speckle in ultrasound b-scans," *IEEE Trans. Sonics Ultrason.*, vol. 30, no. 3, pp. 156–163, 1983.

[3] V. Dutt and J. Greenleaf, "Adaptive speckle reduction filter for log-compressed b-scan images," *IEEE Trans. Med. Imag.*, vol. 15, no. 6, pp. 802–813, 1996.

[4] A. Evans and M. Nixon, "Biased motion-adaptive temporal filtering for speckle reduction in echocardiography," *IEEE Trans. Med. Imag.*, vol. 15, no. 1, pp. 39–50, 1996.

[5] G. Xiao, M. Brady, J. A. Noble, and Y. Zhang, "Segmentation of ultrasound B-mode images with intensity inhomogeneity correction," *IEEE Trans. Med. Imag.*, vol. 21, no. 1, pp. 48–57, 2002.

[6] J. G. Bosch, S. C. Mitchell, B. P. F. Lelieveldt, F. Nijland, O. Kamp, M. Sonka, and J. H. C. Reiber, "Automatic segmentation of echocardiographic sequences by active appearance motion models," *IEEE Trans. Med. Imag.*, vol. 21, no. 11, pp. 1374–1383, 2002.

[7] M. Kass, A. P. Witkin, and D. Terzopoulos, "Snakes: Active contour models," *International Journal of Computer Vision*, vol. 1, no. 4, pp. 321–331, 1988.

[8] A. Sarti, C. Corsi, E. Mazzini, and C. Lamberti, "Maximum likelihood segmentation of ultrasound images with rayleigh distribution," *IEEE Trans. Ultrason.*, vol. 52, no. 6, pp. 974–960, 2005.

[9] Z. Tao and H. D. Tagare, "Tunneling descent for m.a.p. active contours in ultrasound segmentation," *Medical Image Analysis*, vol. 11, no. 3, pp. 266–281, 2007.

[10] M. Mulet-Parada and J. A. Noble, "2D+T acoustic boundary detection in echocardiography," *Medical Image Analysis*, vol. 4, no. 1, pp. 21–30, 2000.

[11] K. Rajpoot, A. Noble, V. Grau, and N. Rajpoot, "Feature detection from echocardiography images using local phase information," in *Proceedings 12th Medical Image Understanding and Analysis (MIUA'2008)*, 2008.

[12] M. Felsberg and G. Sommer, "The monogenic signal," *IEEE Transactions on Signal Processing*, vol. 49, no. 12, pp. 3136–3144, 2001.

[13] A. Belaid, D. Boukerroui, Y. Maingourd, and J.-F. Lerallut, "Phase-based level set segmentation of ultrasound images," *IEEE Transactions on Information Technology in Biomedicine*, vol. 15, no. 1, pp. 138–147, 2011.

[14] E. Ashton and K. Parker, "Multiple resolution bayesian segmentation of ultrasound images," *Ultrason. Imag.*, vol. 17, no. 4, pp. 291–304, 1995.

[15] N. Lin, W. Yu, and J. S. Duncan, "Combinative multi-scale level set framework for echocardiographic image segmentation," *Medical Image Analysis*, vol. 7, no. 4, pp. 529–537, 2003.

[16] T. F. Chan and L. A. Vese, "Active contours without edges," *IEEE Trans. Imag. Proc.*, vol. 10, no. 2, pp. 266–277, 2001.

[17] S. Lankton and A. Tannenbaum, "Localizing region-based active contours," *IEEE Transactions on Image Processing*, vol. 17, no. 11, pp. 2029–2039, 2008.

[18] L. Wang, L. He, A. Mishra, and C. Li, "Active contours driven by local gaussian distribution fitting energy," *Signal Processing*, vol. 89, no. 12, pp. 2435–2447, 2009.

[19] C. Li, C. Xu, C. Gui, and M. D. Fox, "Level set evolution without re-initialization: A new variational formulation," in *CVPR*. IEEE Computer Society, 2005, pp. 430–436.

[20] V. Caselles, R. Kimmel, and G. Sapiro, "Geodesic active contours," *International Journal of Computer Vision*, vol. 22, no. 1, pp. 61–79, 1997.

[21] M. Felsberg and G. Sommer, "A new extension of linear signal processing for estimating local properties and detecting features," in *Proc. 22nd DAGM Symp. Mustererkennung*, 2000, pp. 195–202.

[22] D. Boukerroui, J. A. Noble, and M. Brady, "On the choice of band-pass quadrature filters," *Journal of Mathematical Imaging and Vision*, vol. 21, no. 1-2, pp. 53–80, 2004.

[23] M. C. Morrone and R. A. Owens, "Feature detection from local energy," *Pattern Recogn. Lett.*, vol. 6, no. 5, pp. 303–313, Dec. 1987.

[24] P. Kovesi, "Image features from phase congruency," *Videre*, vol. 1, no. 3, 1999.

[25] L. R. Dice, "Measures of the amount of ecologic association between species," *Ecology*, vol. 26, no. 3, pp. 297–302, July 1945.